

# Structure-Based Identification of Inhibitors for the SLC13 Family of $\text{Na}^+$ /Dicarboxylate Cotransporters

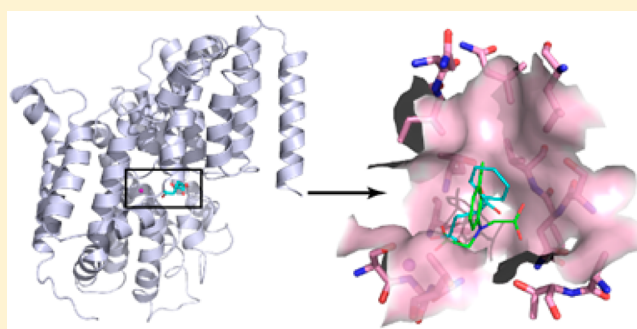
Claire Colas,<sup>†</sup> Ana M. Pajor,<sup>\*,‡</sup> and Avner Schlessinger<sup>\*,†</sup>

<sup>†</sup>Department of Pharmacology and Systems Therapeutics, Tisch Cancer Institute, Icahn School of Medicine at Mount Sinai, New York, New York 10029, United States

<sup>‡</sup>Skaggs School of Pharmacy and Pharmaceutical Sciences, University of California—San Diego, La Jolla, California 92130-0718, United States

## S Supporting Information

**ABSTRACT:** In mammals, citric acid cycle intermediates play a key role in regulating various metabolic processes, such as fatty acid synthesis and glycolysis. Members of the sodium-dependent SLC13 transporter family mediate the transport of di- and tricarboxylates into cells. SLC13 family members have been implicated in lifespan extension and resistance to high-fat diets; thus, they are emerging drug targets for aging and metabolic disorders. We previously characterized key structural determinants of substrate and cation binding for the human NaDC3/SLC13A3 transporter using a homology model. Here, we combine computational modeling and virtual screening with functional and biochemical testing, to identify nine previously unknown inhibitors for multiple members of the SLC13 family from human and mouse. Our results reveal previously unknown substrate selectivity determinants for the SLC13 family, including key residues that mediate ligand binding and transport, as well as promiscuous and specific SLC13 small molecule ligands. The newly discovered ligands can serve as chemical tools for further characterization of the SLC13 family or as lead molecules for the future development of potent inhibitors for the treatment of metabolic diseases and aging. Our results improve our understanding of the structural components that are important for substrate specificity in this physiologically important family as well as in other structurally related transport systems.



Citric acid cycle (CAC) intermediates such as succinate, citrate, and malate are involved in regulating a variety of important metabolic processes in mammals, such as fatty acid synthesis and glycolysis.<sup>1–3</sup> For example, citrate is a regulatory signal in the brain for sensing energy and nutrient availability.<sup>3</sup> In humans, the transport of these di- and tricarboxylates across the plasma membrane into cells is mediated through three sodium-dependent transporters of the SLC13 family: hNaDC1 (SLC13A2), hNaDC3 (SLC13A3), and hNaCT (SLC13A5). Reduction of the activity of SLC13 homologues in *Drosophila melanogaster*<sup>4,5</sup> and *Caenorhabditis elegans*<sup>6,7</sup> leads to increased lifespan and reduced fat storage. More recently, deletion of the mouse *slc13a5* gene (mNaCT) was shown to cause substantial metabolic changes, increased plasma citrate concentrations, and resistance to the deleterious effects of a high-fat diet.<sup>8</sup> Thus, the SLC13 family members are emerging drug targets for metabolic disorders and aging.

The SLC13 family members have diverse tissue distribution and substrate specificities.<sup>9</sup> For example, hNaDC1, found primarily in the renal proximal tubule and small intestine, is a low-affinity transporter ( $K_m$  for succinate is 0.5 mM) of di- and tricarboxylates ranging from four- to six-carbon molecules (e.g., succinate and citrate, respectively).<sup>10</sup> Conversely, hNaDC3 is expressed in multiple tissues, including the kidney (basolateral

membrane), liver, placenta, brain, choroid plexus, and eye.<sup>11,12</sup> hNaDC3 is a high-affinity transporter ( $K_m$  for succinate of  $\sim 20 \mu\text{M}$ ) that transports a broader range of substrates than that of hNaDC1, including dicarboxylates with longer or bulkier side chains, as well as drugs such as succimer and the antioxidant glutathione.<sup>13,14</sup> In contrast, the liver and brain  $\text{Na}^+$ /citrate transporter, NaCT, has a narrow substrate specificity with a preference for citrate.<sup>15</sup> The mechanisms underlying the transport of the CAC intermediates, including the structural basis for the differential binding and transport specificity among the SLC13 family members, are poorly understood.

Description of the substrate specificity determinants of the SLC13 transporters includes the identification of structural features such as charge, polarity, and shape on the proteins' surface that determine differential binding and transport of small molecule ligands and ions. There is currently no known experimentally determined atomic structure for any of the human SLC13 family transporters; however, the structure of the bacterial homologue, the sodium-dependent dicarboxylate transporter from *Vibrio cholerae* INDY (vcINDY), has been

Received: April 13, 2015

Revised: July 13, 2015

Published: July 15, 2015

recently determined at atomic resolution.<sup>16</sup> The vcINDY structure, which revealed a novel structural fold, represents an inward open conformation bound to a citrate and a sodium ion and consists of two pseudosymmetrical halves, indicating an “alternating access” transport mechanism, related to other structurally dissimilar transporter families (e.g., LeuT).<sup>17</sup> vcINDY shares sequence identity of 33–35% with the mammalian SLC13 family members and a conserved binding site. Furthermore, functional studies of vcINDY suggest an ion:substrate transport stoichiometry of 3:1, similar to those of hNaDC3 and hNaDC1.<sup>18</sup> Recently, two structures of the same fold have been determined in a similar inward conformation,<sup>19,20</sup> but they are only distantly related to the mammalian SLC13 family (sequence identity of ~15%). Therefore, the vcINDY is the most suitable template for generating homology models of SLC13 transporters from human and mouse. We have previously described a homology model of hNaDC3, which revealed previously unknown structural features important for ligand and ion recognition.<sup>21</sup> Residues that belong to the conserved serine-asparagine-threonine (SNT) motifs were demonstrated by site-directed mutagenesis to mediate substrate and sodium binding in hNaDC3 (e.g., Ser143, Asn144, and Thr485).

In this study, we use a combination of computational prediction and experimental validation to characterize multiple SLC13 family members from human and mouse, providing a more comprehensive description of the specificity determinants in this family. We constructed homology models of human NaDC1 (hNaDC1), mouse NaDC1 (mNaDC1), mouse NaDC3 (mNaDC3), and human NaCT (hNaCT) and used virtual screening of various small molecule libraries to predict inhibitors of these proteins. The top-scoring hits were then tested experimentally using uptake kinetic measurements in cells. Finally, we discuss how the results of the study improve our understanding of the structural basis for substrate selectivity among members of the SLC13 family and can promote the development of potential effective drugs targeting SLC13 family members.

## MATERIALS AND METHODS

**Homology Modeling.** We modeled four SLC13 family transporters (hNaDC1, mNaDC1, mNaDC3, and hNaCT), based on the X-ray structure of vcINDY (Protein Data Bank entry 4F35).<sup>16</sup> We relied on a previously published alignment between hNaDC3 and vcINDY<sup>21</sup> and aligned the other SLC13 family members on the basis of multiple-sequence alignment generated using the PROMALS3D server.<sup>22</sup> We used MODELLER-9v14 to build 100 initial models for each target, which were assessed and ranked by the statistical potential Z-DOPE.<sup>23</sup> The models were built with nonprotein atoms that were derived from the corresponding coordinates of the vcINDY structure. These nonprotein atoms included a sodium ion (Na<sup>+</sup>), as well as atoms from citrate, a weak inhibitor of this protein.<sup>16</sup> Moreover, although a second cation binding site has been previously proposed to be located in close proximity of the ligand,<sup>16</sup> it has not been determined whether both ions are bound with high affinity in this conformation of vcINDY. In fact, in vcINDY, it has been suggested that this conformation represents a state in which the second cation has already been released in the cytoplasm.<sup>16</sup> Taken together, we hypothesized that models of human SLC13 family members in this conformation are suitable for identifying new ligands via virtual screening. While other useful conformational states can be

modeled using a variety of approaches such as relying on the pseudosymmetry of the protein,<sup>24</sup> such models are less likely to be sufficiently accurate for structure-based ligand discovery.<sup>25</sup>

The highest-ranked models yielded Z-DOPE values ranging from −0.27 to −0.12, suggesting that 50–55% of their Ca atoms are within 3.5 Å of their correct positions.<sup>26</sup> These top-scoring models were visually inspected in view of previous studies characterizing structure–function relationships among SLC13 family members.<sup>9</sup> Finally, the side chain of Thr236 of the mNaDC1 model was refined with Chimera<sup>27</sup> to face the binding pocket.

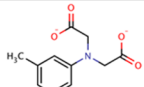
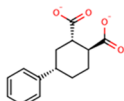
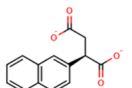
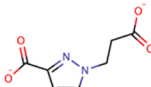
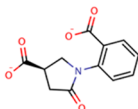
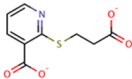
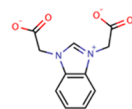
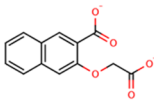
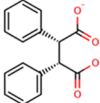
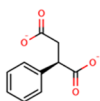
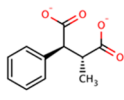
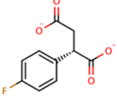
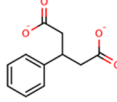
**Virtual Screening.** OpenEye FRED (Fast Rigid Exhaustive Docking)<sup>28</sup> was used for all docking calculations. The transporter’s binding site was prepared with the MAKE\_RECEPTOR utility. We defined a box enclosing the binding site around the coordinates of the citrate derived from the X-ray structure of vcINDY, and the sodium ion was defined as part of the binding site.<sup>16</sup> The docking poses were evaluated by the Chemgauss4 scoring function, which is based on the shape and chemical complementarity between the ligands and the binding site.<sup>28</sup> We docked three subsets from the ZINC database,<sup>41</sup> the “Drugs Now”, “Leads Now”, and “Fragments Now” subsets (2726001 compounds in total), against the hNaDC1 and hNaDC3 models and prioritized molecules for experimental testing based on visual analysis (text of the [Supporting Information](#)).

Briefly, we compared the docking poses of the top 500 scoring compounds of each screen to those of known ligands in the models, as well as to the mode of interaction of citrate in the experimentally determined structure of vcINDY (Figure 1).<sup>16</sup> In brief, eight molecules were initially tested [1–8 (Table 1)] based on the following considerations. (i) We favored dicarboxylate compounds interacting with the N- or C-terminal SNT motifs, which are highly important for function.<sup>9,21,29</sup> (ii) Moreover, to explore nontrivial ligands and previously unknown modes of interaction with the transporters, we prioritized molecules that are predicted to interact with other key binding site residues. For example, Thr527 of hNaDC3 was suggested to participate in a network of interactions involving the substrate and a putative second Na<sup>+</sup> ion.<sup>21</sup> (iii) Finally, we selected molecules that contain novel chemical groups (e.g., aromatic rings). For example, molecules 1 and 3 included a toluene and a naphthalene group, respectively, that were predicted to form a hydrophobic interaction with a hydrophobic subpocket in hNaDC3 (constituted by helices TM9b, TM5b, and HP<sub>out</sub>) (Figure 3A). The selected compounds were then also docked in the mouse models.

**Cell Culture.** Human embryonic kidney (HEK-293) cells (CRL-1573, American Type Culture Collection, Manassas, VA) were cultured in Dulbecco’s modified Eagle’s medium (DMEM) supplemented with 25 mM HEPES, 2 mM Glutamax, 1 mM sodium pyruvate, 0.1 mM nonessential amino acids, 10% heat-inactivated fetal calf serum, 100 units/mL penicillin, and 100 µg/mL streptomycin at 37 °C in 5% CO<sub>2</sub>.<sup>30</sup> Cells were plated on poly-D-lysine-coated 96-well plates (BD Biosciences, San Jose, CA) at a density of 0.6 × 10<sup>5</sup> cells per well and transfected with plasmids encoding SLC13 transporters using FuGene6 (Roche Applied Science, Indianapolis, IN) at a 3:1 ratio.

**Transport Assays.** Uptake of 2,3-[<sup>14</sup>C]succinate (52 mCi/mmol) or 1,5-[<sup>14</sup>C]citrate (112 mCi/mmol) (both from Moravsek, La Brea, CA) was assayed 48 h after transfection, also as described previously.<sup>30</sup> The [<sup>14</sup>C]citrate was used for the

**Table 1. Top-Scoring Compounds Tested in Uptake Experiments**

Compound <sup>a</sup>	Rank <sup>b,c</sup>	Sketch <sup>d</sup>
1	500+, 20	
2	500+, 33	
3	500+, 50	
4	500+, 80	
5	3, 1	
6	26, 93	
7	311, 178	
8	379, 40	
9	500+, 500+	
10	500+, 500+	
11	500+, 500+	
12	500+, 500+	
13	500+, 500+	

<sup>a</sup>The Compound column lists the number for each molecule. <sup>b,c</sup>The Rank column lists the rank of the compound within the virtual screening against the hNaDC1 (b) and hNaDC3 (c) models; 500+ indicates that the compound was not ranked within the 500 best scored compounds visually analyzed. <sup>d</sup>The Sketch column lists the two-dimensional structure of the molecule.

citrate transporter, NaCT, because of low succinate transport activity. The sodium transport buffer consisted of 140 mM NaCl, 2 mM KCl, 1 mM MgCl<sub>2</sub>, 1 mM CaCl<sub>2</sub>, and 10 mM HEPES (pH adjusted to 7.4 with 1 M Tris). Choline buffer

contained equimolar choline chloride in place of NaCl. For the assays, each well was washed twice with choline buffer and then incubated with 50  $\mu$ L of sodium buffer containing  $\sim 10$   $\mu$ M [<sup>14</sup>C]succinate or [<sup>14</sup>C]citrate for 30 min at room temperature. The uptake assays were stopped, and surface radioactivity was removed with 4  $\times$  1 mL washes of choline buffer. Cells were dissolved using Ultima Gold scintillation cocktail (PerkinElmer), and then the plates were counted directly using a Wallac Microbeta plate scintillation counter. For all experiments, counts in vector-transfected cells were subtracted from counts in SLC13 plasmid-transfected cells to correct for background.

Initial screens of inhibitors were conducted using concentrations of 500  $\mu$ M. The inhibitor stock solutions were made up to 50 mM in DMSO, and control groups received DMSO only. The final concentration of DMSO was 1%. For subsequent measurements of IC<sub>50</sub> values, a range of stock solutions was made so that equal volumes of DMSO were added to each well. For the initial screen, all inhibitors were preincubated for 12 min in sodium buffer; then plates were washed, and radioactive solution with inhibitor was added.<sup>31</sup> However, we found that inhibition does not require preincubation (results not shown), and therefore, subsequent IC<sub>50</sub> measurements were done without the preincubation. IC<sub>50</sub> values were determined by fitting the data to a four-part logistic curve (SigmaPlot 10.0, Systat Software Inc., San Jose, CA).

**Statistics.** Duplicate or quadruplicate measurements were made for each data point. The experiments were repeated with at least three different batches of transfected cells from different passage numbers. Significant differences between groups were identified by Student's *t* test or analysis of variance with *P* < 0.05.

**Chemicals.** All of the compounds were purchased from commercial vendors. Compounds 1, 5, 6, and 12 were from ChemBridge (San Diego, CA). Compounds 2 and 4 were from Vitas-M-lab (Narva, Estonia). Compounds 3, 10, 11, and 13 were from Sigma-Aldrich (St. Louis, MO). Compound 7 was from Matrix Scientific (Columbia, SC). Compounds 8 and 9 were from Enamine (Ukraine).

## RESULTS

**Structural Models of the SLC13 Family Members.** The models of hNaDC1, mNaDC1, and mNaDC3 were built using MODELLER, based on the X-ray structure of vcINDY as a template<sup>16</sup> (Figure 1) (Materials and Methods), similar to that of our previously described hNaDC3 model.<sup>21</sup> The vcINDY template structure represents an inward open conformation of the transporter bound to citrate, a weak inhibitor of this protein. Notably, previous studies proposed that vcINDY transports solutes via an elevator-type mechanism similar to that of Glt<sub>ph</sub>,<sup>18</sup> suggesting that the structure of the substrate binding pocket is similar in distinct conformational states of the transporter. Indeed, our previous study confirmed that substrate binding residues predicted from this conformation affect transport activity.<sup>21</sup>

The SLC13 models consist of the entire transmembrane domain of the proteins, including 11 helices and two hairpin loops, termed HP<sub>in</sub> and HP<sub>out</sub>. The tips of these hairpins support two serine-asparagine-threonine (SNT) motifs that interact with the substrate and at least one Na<sup>+</sup> ion. These SNT motifs, as well as the majority of the other binding site residues, are highly conserved within the SLC13 family, with some variations in the following two positions (Table 1). Position 1 is located in close proximity of the C-terminal SNT motif, and it



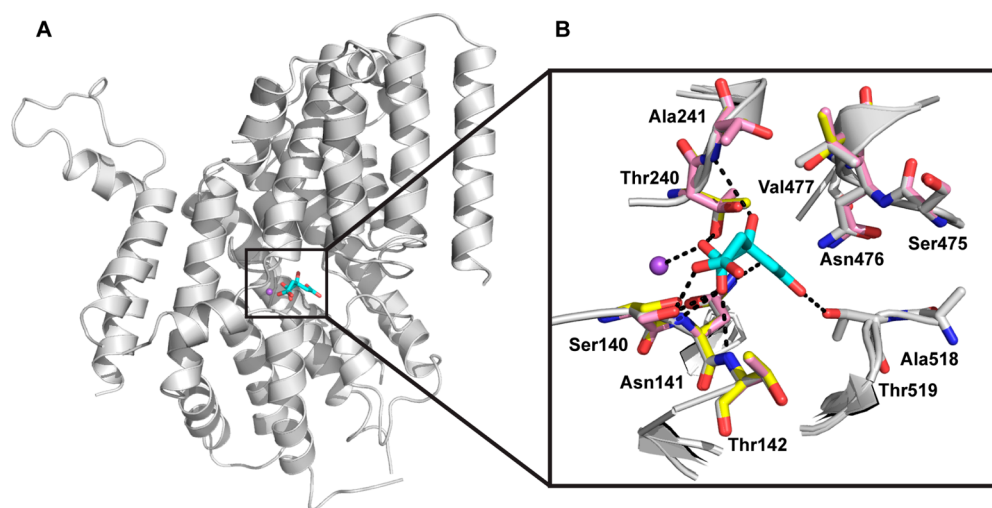


**Figure 1.** Homology models of the SLC13 transporters. (A) Docking pose of the known substrate citrate into the human NaDC1 (hNaDC1) homology model. The backbone atoms of hNaDC1 are visualized as a white cartoon, and the ligand is shown as cyan sticks, with oxygen and nitrogen atoms colored red and blue, respectively. The position of the sodium ion is derived from the model and represented as a purple sphere. (B) Comparison of the binding sites of the SLC13 transporters with hNaDC1 shown as white sticks, the mouse NaDC1 as pink sticks, and human NaDC3 as yellow sticks, with oxygen and nitrogen atoms colored red and blue, respectively. The hNaDC1 residues of the binding site are labeled, and the position of the sodium ion derived from the model is represented as a purple sphere.

can be an alanine (in hNaDC1, hNaDC3, and mNaDC3), a glycine (hNaCT), or a threonine (mNaDC1). Position 2 is the third residue of the C-terminal SNT motif and can be a threonine, a valine, or a glycine.

**Ligand Identification.** We initially used OpenEye FRED to dock the substrate citrate against the hNaDC1 model (Figure 1), to guide ligand discovery with virtual screening. Similarly to citrate in the vCINDY structure, the carboxylate moieties of citrate are predicted to interact with the N-terminal SNT motif of hNaDC1 by forming hydrogen bonds with backbone atoms of Asn141 and Thr142, as well as with the hydroxyl moiety of the Ser140 side chain. Citrate is also coordinated by the side chain hydroxyl of Thr519, the backbone nitrogen of Ala241, and  $\text{Na}^+$ . The close similarity between the binding mode of citrate in the vCINDY crystal structure and the predicted binding mode of this weak inhibitor in the hNaDC1 model suggests that our models can predict binding of substrates or competitive inhibitors with substrate-like structures. We then virtually screened 2726001 compounds from various libraries of the ZINC database (Materials and Methods and Supporting Information); 500 top-scoring hits from the various screens against the models of hNaDC1 and hNaDC3 were prioritized for experimental testing by visual analysis. In particular, top docking poses were inspected for erroneously docked molecules, which can be observed in large virtual screenings, to remove molecules with incorrect ionization states, tautomers, or strained conformations.<sup>32,33</sup> We then selected an initial set of eight molecules [compounds 1–8 (Table 1)], based on their availability and the presence of a unique chemical structure, as well as their interaction with confirmed key binding site residues, such as Ser143, Asn144, Thr245, and Thr485 in hNaDC3. These molecules contained dicarboxylates connected to various scaffolds. For example, compounds 2 and 4–8 contain five- or six-sided rings, and compounds 1, 4, 5, and 8 contain a nitrogen atom in a linear chain.

We tested the transport inhibition by the predicted ligands in a cis-inhibition assay against representative members of the

SLC13 family, human NaDC1, NaDC3, and NaCT, as well as mouse NaDC1 and NaDC3. The transport substrates were [ $^{14}\text{C}$ ]succinate for NaDC1 and NaDC3 (both human and mouse) and [ $^{14}\text{C}$ ]citrate for the citrate transporter, NaCT. Four of the eight tested compounds (compounds 1, 3, 6, and 8) significantly inhibited transport in at least one SLC13 family member (Figure 2 and Figure S1 of the Supporting Information). Moreover, compound 1 inhibited  $^{14}\text{C}$ -labeled substrate transport activity in all transporters, except for NaCT

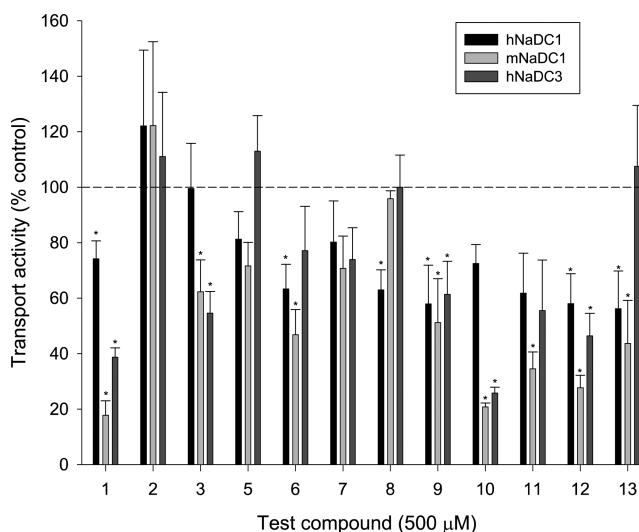


**Figure 2.** Experimental testing of predicted SLC13 inhibitors. HEK-293 cells expressing the following transporters were cultured in 96-well plates: human (h) or mouse (m) NaDC1 and hNaDC3. The cis-inhibition of  $\sim 10 \mu\text{M}$  [ $^{14}\text{C}$ ]succinate transport was measured with a test compound concentration of  $500 \mu\text{M}$ , expressed as a percentage of transport in the absence of test compound (DMSO only). Error bars show the standard error of the mean (SEM) ( $n = 3$ –10 independent experiments). \*Denotes a significant difference from control ( $P < 0.05$ ). The dotted line indicates the position of 100%. Compound 4 had inconsistent effects and is not shown.

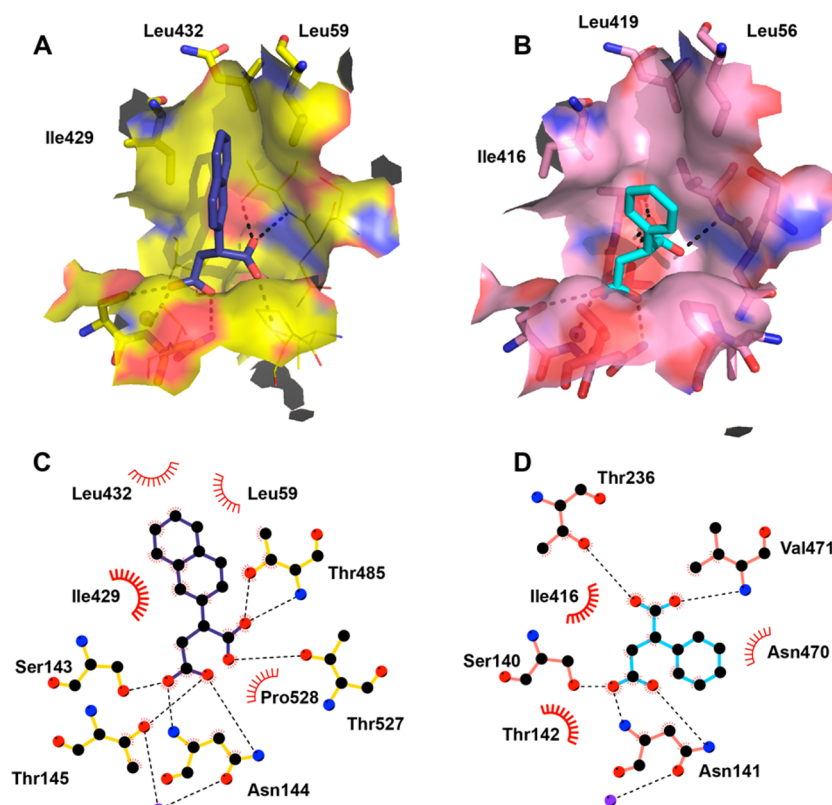


**Figure 3.** Mode of binding of newly discovered ligands. Docking poses of compounds 3 (A and C) and 1 (B and D) with the hNaDC3 and mNaDC1 binding sites, respectively. The top panels show the hNaDC3 (A) and mNaDC1 (B) binding sites in yellow and pink transparent surfaces, respectively. The bottom panels show the binding pose in a two-dimensional representation generated by ligplot,<sup>40</sup> where the hNaDC3 (A) and mNaDC1 (B) residues forming hydrogen bonds with the ligands are colored yellow and pink, respectively, and the residues establishing hydrophobic interactions are shown as red spoked arcs. Compounds 3 and 10 are visualized as blue and cyan sticks, respectively.

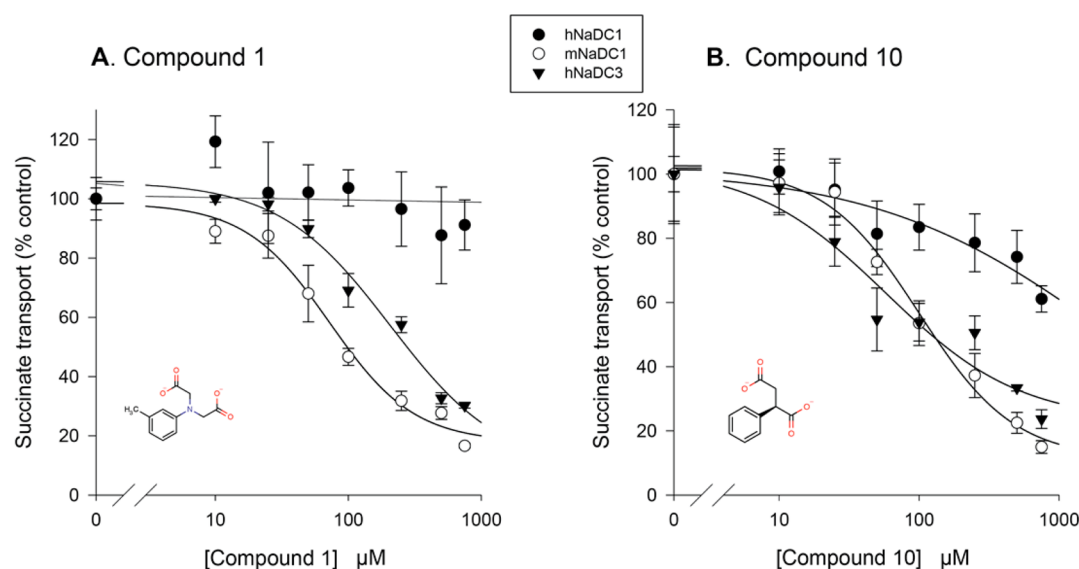


**Figure 4.** Concentration dependence of inhibition of SLC13 transporters by predicted SLC13 inhibitors. Transport of [ $^{14}\text{C}$ ]succinate ( $\sim 10 \mu\text{M}$ ) was measured in the presence and absence of test compound 1 (A) or 10 (B) at concentrations between 10 and  $750 \mu\text{M}$ . HEK-293 cells were transiently transfected with plasmids encoding hNaDC1, mNaDC1, or hNaDC3. The data points are normalized to transport activity in the absence of inhibitor. Error bars represent SEM ( $n = 3$  wells from a single experiment).

(Figure S1 of the [Supporting Information](#)). The sensitivity to inhibition of hNaDC1 by compound 1 was somewhat variable, and at the moment, we do not have an explanation for this. Next, five additional molecules were selected from the ZINC database for experimental testing based on their similarity to

our most potent hit compound 1 [compounds 9–13 ([Table 1](#))]. These compounds were selected to refine the newly discovered scaffold of compound 1, even though they were not necessarily ranked within the 500 top-scoring compounds of each screen ([Table 1](#)). Specifically, we focused on compounds

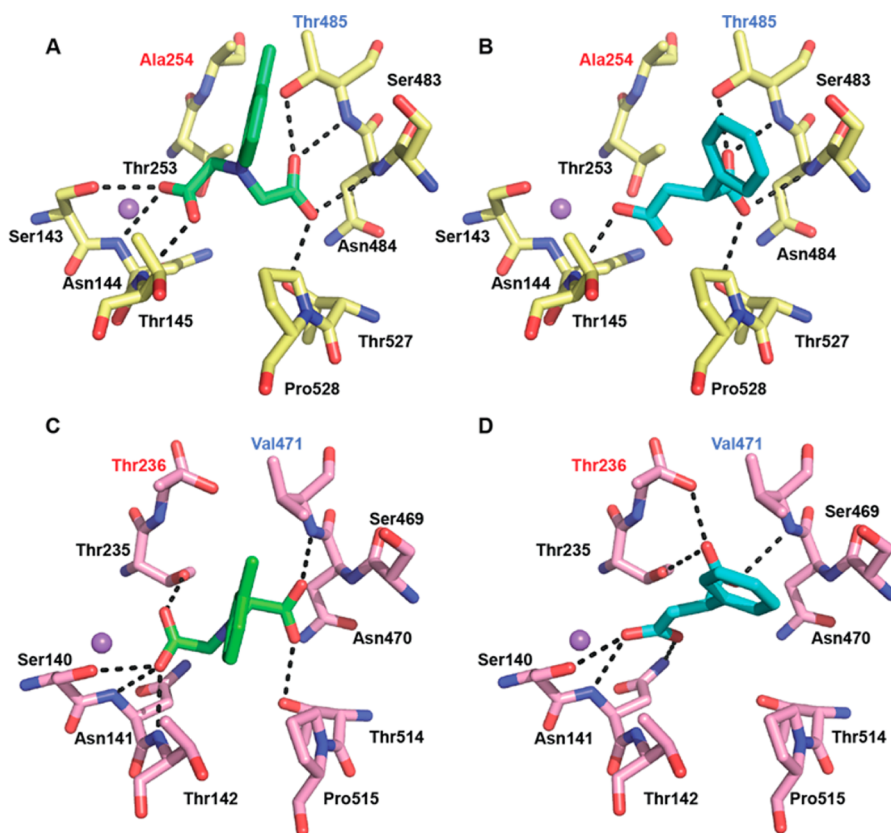


**Figure 5.** Predicted ligand binding mode for hNaDC3 and mNaDC1. Docking poses of compounds **1** (A and C) and **10** (B and D) represented in hNaDC3 (yellow) and mNaDC1 (pink), respectively. Compounds **1** and **10** are colored green and cyan, respectively, with oxygen atoms colored red and nitrogen atoms blue. Residues defining substitutions 1 and 2 (Table 1) are labeled in red and blue, respectively.

with varying carbon chain lengths and diverse substituent sizes. For example, both **10** and **3** have benzene as a substituent, but the chains are four and five carbons long, respectively; both **6** and **11** have four carbon chains and two substituents, either two benzenes (**6**) or a benzene and a methyl group (**11**). All five compounds (**9–13**) inhibited at least one SLC13 family member, with **10** being the most potent. Interestingly, hNaCT, which interacts with tricarboxylates such as citrate and exhibits unique substrate:cation stoichiometry (i.e., it binds four sodium ions), was significantly inhibited by compound **12**, a dicarboxylate with an aromatic moiety (Table 1 and Figure S1 of the Supporting Information).

**Analysis of Inhibitors.** On the basis of the cis-inhibition assays, we compared the docking poses of compound **10**, one of the most potent inhibitors, in mNaDC1, and compound **3**, the most selective ligand for hNaDC3 inhibition (Figure 3). Both ligands are predicted to form hydrogen bonds with the conserved N- and C-terminal SNT motifs. Interestingly, subtle differences between the binding sites of these proteins may explain their differential binding specificities. For example, Thr236 in mNaDC1 is substituted by Ala254 in hNaDC3 (Table S1 of the Supporting Information and Figures 3A,B and 4A–D), leading to the formation of an additional subpocket by Leu59, Ile429, and Leu432 in hNaDC3. This subpocket can accommodate the bulky naphthalene moiety of compound **3** (Figure 3A,C). Moreover, in mNaDC1, the side chain of Ile416 faces the binding site, making the corresponding pocket narrower, which limits the interaction with larger and bulkier ligands such as compound **3**.

Next, compounds **1** and **10** were selected for measurements of concentration-dependent inhibition of hNaDC3, hNaDC1, and mNaDC1. These compounds were selected because (i) they were two of the most potent inhibitors among the nine newly identified ligands, (ii) they exhibited some selectivity for specific SLC13 family members (e.g., did not inhibit NaCT), and (iii) they differ in their lengths, where compounds **1** and **10** are five- and four-atom chain dicarboxylates, respectively. mNaDC1 was inhibited by compound **1** with an  $IC_{50}$  value of 72  $\mu$ M (Figure 4A), and in a second experiment (not shown), the  $IC_{50}$  was 82  $\mu$ M. hNaDC3 had higher  $IC_{50}$  values compared with mNaDC1 [207  $\mu$ M (Figure 4A)], and in four experiments,  $159 \pm 41$   $\mu$ M). In contrast, hNaDC1 was insensitive to inhibition by compound **1** (Figure 4A). The results with compound **10** were similar to those with compound **1**. The  $IC_{50}$  values for compound **10** were as follows: mNaDC1 [85  $\mu$ M (Figure 4B) and 100  $\mu$ M, second experiment] and hNaDC3 [59  $\mu$ M (Figure 4B)], and the mean of four experiments was  $82 \pm 14$   $\mu$ M]. hNaDC1 was poorly inhibited by compound **10**, with an estimated  $IC_{50}$  of  $\sim$ 2 mM. The  $IC_{50}$  values for mNaDC1 and hNaDC3 are similar to their succinate  $K_m$  values.<sup>34,35</sup>

Next, we compared the predicted complexes of hNaDC3 and mNaDC1 with compounds **1** and **10**. Compound **1** adopts different binding modes in the two transporter/ligand complexes (Figure 5). In the hNaDC3 complex, compound **1** forms hydrogen bonds with side chain atoms of the N- and C-terminal SNT motif residues and van der Waals contacts in a hydrophobic subpocket, which is unique to this transporter (Figure 3A,C). Conversely, because the third position of the C-



terminal SNT motif in mNaDC1 is occupied by a valine residue [Val471 (Table S1 of the [Supporting Information](#))], compound **1** interacts with the backbone atoms of the C-terminal SNT motif of this protein. Compound **10** exhibits a similar differential mode of interaction across the two transporters, with one key difference. Compound **10** forms a hydrogen bond with the side chain of Thr236 in mNaDC1, which is specific to this transporter ([Figure 5D](#) and Table S1 of the [Supporting Information](#)). In summary, these newly identified inhibitors exhibited IC<sub>50</sub> values in the micromolar range and some selectivity, providing important chemical tools for further study of these transporters. Although not all the different specificities can be explained structurally at this point, the IC<sub>50</sub> values indicate that these newly discovered ligands can be physiologically and clinically relevant for membrane transporters found in the liver and kidney.<sup>9,36</sup>

## DISCUSSION

Cellular concentrations of citric acid cycle (CAC) metabolites are partly determined by the activity of the SLC13 family of Na<sup>+</sup>-coupled di- and tricarboxylate transporters. Understanding the mechanisms of transport by this family is required for further characterization of their physiological roles, as well as for developing drugs against metabolic disorders and aging. A key step toward describing the substrate specificity among the members of the SLC13 family includes structural characterization of these proteins, the identification of structure–function relationships within the family, and the discovery of novel, specific small molecule ligands for each. In this study, we took a modeling-based approach to identify new inhibitors of the SLC13 family, which represents an alternative to large-scale labor intensive inhibitor screens. This approach has been used successfully to identify ligands for several other transporters such as NET,<sup>37</sup> GAT-2,<sup>38</sup> and LAT-1.<sup>39</sup> Here we modeled mammalian SLC13 family members based on an inward conformation of vINDY, the closest representative atomic resolution structure of this structural family. Although outward-facing conformations can potentially be even more useful for inhibitor discovery, it has been previously proposed that vINDY is an elevator-type transporter,<sup>18</sup> in which the geometry of the binding site is similar for the different states of the transport cycle. This hypothesis is reinforced by our successful identification of inhibitors based on the inward-facing models in this study.

Three key results are presented in this study. First, small molecule ligands for five SLC13 family members from human and mouse (i.e., hNaDC1, mNaDC1, hNaDC3, mNaDC3, and hNaCT) were identified at a high hit rate from structure-based virtual screening ([Figure 2](#), [Figure S1](#) of the [Supporting Information](#), and [Table 1](#)). This finding provides novel chemical tools to further characterize the cellular functions of these transporters. Second, optimization of the initial small molecule hits suggests that differential ligand binding specificity among SLC13 family members is largely determined by the length of the carbon chain and size of the dicarboxylates ([Table 1](#) and [Figures 2–4](#)). This result provides preliminary tools for designing more specific chemical probes to further characterize the SLC13 family members and identifies lead-like molecules for future drug development. Third, systematic application of homology modeling of multiple SLC13 family members, followed by ligand docking and experimental testing, as well as a comparison of their mode of interactions with their ligands, revealed key residues for function and selectivity ([Figures 1, 3,](#)

and [4](#) and [Table S1](#) of the [Supporting Information](#)). This result visualizes key specificity determinants for this important family for the first time such as subpockets that can be targeted for the design of specific ligands. We now discuss each of the three findings in turn.

The first key finding from this study is the identification of novel, specific small molecule inhibitors for SLC13 family members. All the newly discovered inhibitors contain aromatic rings that can be involved in previously uncharacterized interactions with hydrophobic binding site residues [e.g., with Leu59, Leu429, and Leu432 in hNaDC3 ([Figure 3A,C](#))]. Because SLC13 family members exhibit high substrate specificity, almost any change in the structure of a test compound may have large effects. Our results indicate the complexity of how ligand specificity is obtained in this family, where small changes on the binding site surface can shift the ligand preference. Notably, the newly identified inhibitors interact with SLC13 family members with IC<sub>50</sub> values in the micromolar range, similar to physiological concentrations of substrates.<sup>36</sup> At present, we do not know if the inhibitors only bind to the transporters or if they are transported themselves.

The second key result from this study is the optimization of our initial promiscuous hit (compound **1**) by testing new compounds with varying sizes and carbon chain lengths, which provide chemical features that can be further developed to pharmacophores targeting specific SLC13 family members. Our previous docking of known substrates (e.g., succinate and glutarate) against the hNaDC3 model suggested that such four- or five-carbon dicarboxylates may have various binding modes,<sup>21</sup> which is in agreement with the predicted binding poses of compounds **1** and **10** in mNaDC1 in this study ([Figure 5](#)). For example, docking of compound **10**, with a four-carbon dicarboxylate backbone, to hNaDC3 suggests that it forms hydrogen bonds with Thr485 of the C-terminal SNT motif ([Figure 5](#) and [Table S1](#) of the [Supporting Information](#)). In mNaDC1, this residue is substituted with a valine, and a different residue, Thr236, is predicted to contribute to the interaction with compound **10** by forming new hydrogen bonds with this compound ([Figure 5D](#)). However, molecular docking suggests that compound **1**, with a five-carbon dicarboxylate backbone, is too large to rearrange itself and interact with Thr236. Compound **1** still inhibits mNaDC1, suggesting that the complexity of interaction between small molecules and SLC13 family members is not entirely captured by modeling the inward conformation alone, as well as by using cell-based assays. Furthermore, only compound **12** had an effect on hNaCT, confirming the different inhibitor binding specificity of this transporter compared to those of the other members of the family.<sup>30</sup> These new ligands highlight the complexity of how the SLC13 family members achieve their substrate specificity; despite the high degree of similarity of their structures (they are all dicarboxylates and possess aromatic rings), their inhibition profiles are different. Future elucidation of SLC13 conformations as well as the application of complementary experimental approaches that directly measure binding and transport<sup>18</sup> might explain this differential sensitivity to inhibition.

Third, our SLC13 models bound to previously and newly characterized ligands highlight two key positions that define a unique binding site in each SLC13 family member, thereby providing a framework for rationalizing substrate specificity among the SLC13 family members ([Table S1](#) of the [Supporting Information](#)). Position 1 is located in close proximity of the C-terminal SNT motif ([Figures 1](#) and [5](#)). For example, in

hNaDC3, this residue (Ala254) contributes to the formation of an additional hydrophobic subpocket specific to this protein that can accommodate bulkier ligands such as compound 3 (Figure 3A,C). Position 2 is the third residue of the C-terminal SNT motif, and it has some variability among the SLC13 family members; it is occupied by a threonine residue in vINDY and NaDC3 (both human and mouse) or by a valine residue in NaDC1 (both human and mouse) and NaCT. As described in this study, this residue is likely to play a key role in interaction with ligands.

In conclusion, it is plausible that the combined differences among the transporters, although subtle, affect the overall hydrophobicity and shape of their corresponding binding sites, which is reflected in the binding specificities of their ligands. Some differences in inhibitor specificity among hNaDC3, mNaDC3, hNaDC1, and hNaCT could not be rationalized by the models. Thus, future experimental and computational characterization of SLC13 family members and their homologues in additional conformations is likely to contribute to our understanding of transport mechanisms in this family. Taken together, this study shows the feasibility of using structure-based approaches to identify potential inhibitors of the SLC13 family and highlights the necessity of subsequent experimental verification. These findings are expected to inform future development of drugs targeting this family of transporters.

## ■ ASSOCIATED CONTENT

### ■ Supporting Information

Ligand libraries for virtual screening, Figure S1, and Table S1. The Supporting Information is available free of charge on the ACS Publications website at DOI: 10.1021/acs.biochem.5b00388.

## ■ AUTHOR INFORMATION

### Corresponding Authors

\*E-mail: avner.schlessinger@mssm.edu.

\*E-mail: apajor@ucsd.edu.

### Funding

This work was supported in part by National Institutes of Health Grant R01 GM108911.

### Notes

The authors declare no competing financial interest.

## ■ ACKNOWLEDGMENTS

We thank P. M. Ung for technical assistance and maintenance of the computational resources required for this study. Thanks to D. Rozenshteyn for assistance with the inhibition experiments. This work was supported in part by the computational resources and staff expertise provided by the Department of Scientific Computing at the Icahn School of Medicine at Mount Sinai. We appreciate OpenEye Scientific Software Inc. for granting us access to its high-performance molecular modeling applications through its academic license program.

## ■ ABBREVIATIONS

SLC, solute carrier.

## ■ REFERENCES

- (1) Gullans, S. R.; Kone, B. C.; Avison, M. J.; and Giebisch, G. (1988) Succinate alters respiration, membrane potential, and intracellular K<sup>+</sup> in proximal tubule. *Am. J. Physiol.* 255, F1170–1177.
- (2) Ruderman, N. B., Saha, A. K., Vavvas, D., and Witters, L. A. (1999) Malonyl-CoA, fuel sensing, and insulin resistance. *Am. J. Physiol.* 276, E1–E18.
- (3) Stoppa, G. R., Cesquini, M., Roman, E. A., Prada, P. O., Torsoni, A. S., Romanatto, T., Saad, M. J., Velloso, L. A., and Torsoni, M. A. (2008) Intracerebroventricular injection of citrate inhibits hypothalamic AMPK and modulates feeding behavior and peripheral insulin signaling. *J. Endocrinol.* 198, 157–168.
- (4) Rogina, B., Reenan, R. A., Nilsen, S. P., and Helfand, S. L. (2000) Extended life-span conferred by cotransporter gene mutations in *Drosophila*. *Science* 290, 2137–2140.
- (5) Wang, P. Y., Neretti, N., Whitaker, R., Hosier, S., Chang, C., Lu, D., Rogina, B., and Helfand, S. L. (2009) Long-lived Indy and calorie restriction interact to extend life span. *Proc. Natl. Acad. Sci. U. S. A.* 106, 9262–9267.
- (6) Fei, Y. J., Inoue, K., and Ganapathy, V. (2003) Structural and functional characteristics of two sodium-coupled dicarboxylate transporters (ceNaDC1 and ceNaDC2) from *Caenorhabditis elegans* and their relevance to life span. *J. Biol. Chem.* 278, 6136–6144.
- (7) Fei, Y. J., Liu, J. C., Inoue, K., Zhuang, L., Miyake, K., Miyauchi, S., and Ganapathy, V. (2004) Relevance of NAC-2, an Na<sup>+</sup>-coupled citrate transporter, to life span, body size and fat content in *Caenorhabditis elegans*. *Biochem. J.* 379, 191–198.
- (8) Birkenfeld, A. L., Lee, H. Y., Guebre-Egziabher, F., Alves, T. C., Jurczak, M. J., Jornayvaz, F. R., Zhang, D., Hsiao, J. J., Martin-Montalvo, A., Fischer-Rosinsky, A., Spranger, J., Pfeiffer, A. F., Jordan, J., Fromm, M. F., Konig, J., Lieske, S., Carmean, C. M., Frederick, D. W., Weismann, D., Knauf, F., Irusta, P. M., De Cabo, R., Helfand, S. L., Samuel, V. T., and Shulman, G. I. (2011) Deletion of the mammalian INDY homolog mimics aspects of dietary restriction and protects against adiposity and insulin resistance in mice. *Cell Metab.* 14, 184–195.
- (9) Pajor, A. M. (2014) Sodium-coupled dicarboxylate and citrate transporters from the SLC13 family. *Pfluegers Arch.* 466, 119–130.
- (10) Wright, S. H., Kippen, I., Klinenberg, J. R., and Wright, E. M. (1980) Specificity of the transport system for tricarboxylic acid cycle intermediates in renal brush borders. *J. Membr. Biol.* 57, 73–82.
- (11) Kekuda, R., Wang, H., Huang, W., Pajor, A. M., Leibach, F. H., Devoe, L. D., Prasad, P. D., and Ganapathy, V. (1999) Primary structure and functional characteristics of a mammalian sodium-coupled high affinity dicarboxylate transporter. *J. Biol. Chem.* 274, 3422–3429.
- (12) Pajor, A. M., Gangula, R., and Yao, X. (2001) Cloning and functional characterization of a high-affinity Na<sup>+</sup>/dicarboxylate cotransporter from mouse brain. *Am. J. Physiol.* 280, C1215–C1223.
- (13) Burckhardt, B. C., Drinkuth, B., Menzel, C., Konig, A., Steffen, J., Wright, S. H., and Burckhardt, G. (2002) The renal Na<sup>+</sup>-dependent dicarboxylate transporter, NaDC-3, translocates dimethyl- and disulphydryl-compounds and contributes to renal heavy metal detoxification. *J. Am. Soc. Nephrol.* 13, 2628–2638.
- (14) Schorbach, L., Krick, W., Burckhardt, G., and Burckhardt, B. C. (2013) Glutathione is a low-affinity substrate of the human sodium-dependent dicarboxylate transporter. *Nephron. Physiology* 124, 1–5.
- (15) Inoue, K., Zhuang, L., and Ganapathy, V. (2002) Human Na<sup>+</sup>-coupled citrate transporter: primary structure, genomic organization, and transport function. *Biochem. Biophys. Res. Commun.* 299, 465–471.
- (16) Mancusso, R., Gregorio, G. G., Liu, Q., and Wang, D. N. (2012) Structure and mechanism of a bacterial sodium-dependent dicarboxylate transporter. *Nature* 491, 622–626.
- (17) Forrest, L. R., Kramer, R., and Ziegler, C. (2011) The structural basis of secondary active transport mechanisms. *Biochim. Biophys. Acta, Bioenerg.* 1807, 167–188.
- (18) Mulligan, C., Fitzgerald, G. A., Wang, D. N., and Mindell, J. A. (2014) Functional characterization of a Na<sup>+</sup>-dependent dicarboxylate transporter from *Vibrio cholerae*. *J. Gen. Physiol.* 143, 745–759.
- (19) Bolla, J. R., Su, C. C., Delmar, J. A., Radhakrishnan, A., Kumar, N., Chou, T. H., Long, F., Rajashankar, K. R., and Yu, E. W. (2015) Crystal structure of the *Alcanivorax borkumensis* YdaH transporter reveals an unusual topology. *Nat. Commun.* 6, 6874.



- (20) Su, C. C., Bolla, J. R., Kumar, N., Radhakrishnan, A., Long, F., Delmar, J. A., Chou, T. H., Rajashankar, K. R., Shafer, W. M., and Yu, E. W. (2015) Structure and function of *Neisseria gonorrhoeae* MtrF illuminates a class of antimetabolite efflux pumps. *Cell Rep.* 11, 61–70.
- (21) Schlessinger, A., Sun, N. N., Colas, C., and Pajor, A. M. (2014) Determinants of substrate and cation transport in the human Na<sup>+</sup>/dicarboxylate cotransporter NaDC3. *J. Biol. Chem.* 289, 16998–17008.
- (22) Pei, J., Kim, B. H., and Grishin, N. V. (2008) PROMALS3D: a tool for multiple protein sequence and structure alignments. *Nucleic Acids Res.* 36, 2295–2300.
- (23) Shen, M. Y., and Sali, A. (2006) Statistical potential for assessment and prediction of protein structures. *Protein Sci.* 15, 2507–2524.
- (24) Radestock, S., and Forrest, L. R. (2011) The alternating-access mechanism of MFS transporters arises from inverted-topology repeats. *J. Mol. Biol.* 407, 698–715.
- (25) Schlessinger, A., Yee, S. W., Sali, A., and Giacomini, K. M. (2013) SLC classification: an update. *Clin. Pharmacol. Ther.* 94, 19–23.
- (26) Eramian, D., Eswar, N., Shen, M. Y., and Sali, A. (2008) How well can the accuracy of comparative protein structure models be predicted? *Protein Sci.* 17, 1881–1893.
- (27) Pettersen, E. F., Goddard, T. D., Huang, C. C., Couch, G. S., Greenblatt, D. M., Meng, E. C., and Ferrin, T. E. (2004) UCSF Chimera—a visualization system for exploratory research and analysis. *J. Comput. Chem.* 25, 1605–1612.
- (28) McGann, M. (2011) FRED pose prediction and virtual screening accuracy. *J. Chem. Inf. Model.* 51, 578–596.
- (29) Pajor, A. M., and Randolph, K. M. (2005) Conformationally sensitive residues in extracellular loop 5 of the Na<sup>+</sup>/dicarboxylate cotransporter. *J. Biol. Chem.* 280, 18728–18735.
- (30) Pajor, A. M., and Sun, N. N. (2013) Nonsteroidal anti-inflammatory drugs and other anthranilic acids inhibit the Na<sup>+</sup>/dicarboxylate symporter from *Staphylococcus aureus*. *Biochemistry* 52, 2924–2932.
- (31) Pajor, A. M., and Randolph, K. M. (2007) Inhibition of the Na<sup>+</sup>/dicarboxylate cotransporter by anthranilic acid derivatives. *Molecular pharmacology* 72, 1330–1336.
- (32) Schlessinger, A., Khuri, N., Giacomini, K. M., and Sali, A. (2013) Molecular Modeling and Ligand Docking for Solute Carrier (SLC) Transporters. *Curr. Top. Med. Chem.* 13, 843–856.
- (33) Shoichet, B. K. (2004) Virtual screening of chemical libraries. *Nature* 432, 862–865.
- (34) Burckhardt, B. C., Lorenz, J., Kobbe, C., and Burckhardt, G. (2005) Substrate specificity of the human renal sodium dicarboxylate cotransporter, hNaDC-3, under voltage-clamp conditions. *Am. J. Physiol.* 288, F792–F799.
- (35) Pajor, A. M., and Sun, N. N. (2000) Molecular cloning, chromosomal organization, and functional characterization of a sodium-dicarboxylate cotransporter from mouse kidney. *Am. J. Physiol.* 279, F482–F490.
- (36) Giacomini, K. M., Huang, S. M., Tweedie, D. J., Benet, L. Z., Brouwer, K. L., Chu, X., Dahlin, A., Evers, R., Fischer, V., Hillgren, K. M., Hoffmaster, K. A., Ishikawa, T., Keppler, D., Kim, R. B., Lee, C. A., Niemi, M., Polli, J. W., Sugiyama, Y., Swaan, P. W., Ware, J. A., Wright, S. H., Yee, S. W., Zamek-Gliszczynski, M. J., and Zhang, L. (2010) Membrane transporters in drug development. *Nat. Rev. Drug Discovery* 9, 215–236.
- (37) Schlessinger, A., Geier, E., Fan, H., Irwin, J. J., Shoichet, B. K., Giacomini, K. M., and Sali, A. (2011) Structure-based discovery of prescription drugs that interact with the norepinephrine transporter, NET. *Proc. Natl. Acad. Sci. U. S. A.* 108, 15810–15815.
- (38) Schlessinger, A., Wittwer, M. B., Dahlin, A., Khuri, N., Bonomi, M., Fan, H., Giacomini, K. M., and Sali, A. (2012) High Selectivity of the gamma-Aminobutyric Acid Transporter 2 (GAT-2, SLC6A13) Revealed by Structure-based Approach. *J. Biol. Chem.* 287, 37745–37756.
- (39) Geier, E. G., Schlessinger, A., Fan, H., Gable, J. E., Irwin, J. J., Sali, A., and Giacomini, K. M. (2013) Structure-based ligand discovery for the Large-neutral Amino Acid Transporter 1, LAT-1. *Proc. Natl. Acad. Sci. U. S. A.* 110, 5480–5485.
- (40) Laskowski, R. A., and Swindells, M. B. (2011) LigPlot<sup>+</sup>: multiple ligand-protein interaction diagrams for drug discovery. *J. Chem. Inf. Model.* 51, 2778–2786.
- (41) Irwin, J. J., and Shoichet, B. K. (2005) ZINC—a free database of commercially available compounds for virtual screening. *J. Chem. Inf. Model.* 45, 177–182.